Eur. Phys. J. B **38**, 13–18 (2004)
DOI: 10.1140/epjb/e2004-00093-1

THE EUROPEAN PHYSICAL JOURNAL B

Magnetic properties of the antiferromagnetic site-disordered vanadate $Zn_2FeV_3O_{11}$

V. Likodimos[1], N. Guskos[2,a], S. Glenis[2], R. Szymczak[3], A. Bezkrovnyi[4], M. Wabia[5,†], J. Typek[5], G. Gasiorek[5], M. Kurzawa[6], I. Rychlowska-Himmel[6], and A. Blonska-Tabero[6]

[1] Physics Department, National Technical University, 157 80 Athens, Greece
[2] Department of Physics, University of Athens, 157 84 Zografou, Athens, Greece
[3] Institute of Physics, Polish Academy of Sciences, 02-668 Warsaw, Poland
[4] Frank Laboratory of Neutron Physics, JINR, 141 980 Dubna, Russia
[5] Institute of Physics, Technical University of Szczecin, 71-065 Szczecin, Poland
[6] Institute of Chemistry, Technical University of Szczecin, 71-065 Szczecin, Poland

Received 3 October 2003 / Received in final form 23 December 2003
Published online 20 April 2004 –

Abstract. The magnetic properties of the $Zn_2FeV_3O_{11}$ vanadate, characterized by a disordered distribution of diamagnetic Zn^{2+} and high-spin Fe^{3+} ions, are studied using magnetization and electron paramagnetic resonance (EPR) measurements. The dc susceptibility reveals antiferromagnetic interactions between Fe^{3+} spins with a Curie-Weiss temperature $\Theta = -58(1)$ K, followed by a transition to a frozen, spin-glass-like state at low temperature $T_f \approx 2.55$ K, indicating an inhomogeneous magnetic ground state. The temperature variation of the EPR parameters confirms the antiferromagnetic coupling of Fe^{3+} spins at high temperatures, while a distinct divergence is observed at $T \approx 55$ K. This behavior is attributed to the inherent magnetic inhomogeneity of the system due to antiferromagnetic spin clusters.

PACS. 75.50.Lk Spin glasses and other random magnets – 75.50.Ee Antiferromagnetics – 76.30.-v Electron paramagnetic resonance and relaxation

1 Introduction

Site disorder and frustration, frequently occurring in transition metal oxides, may lead to a highly degenerate ground state that hinders long-range order [1]. Prominent examples are provided by spin glasses [2] and geometrically frustrated antiferromagnets, where all spin interactions can not be simultaneously minimized due to lattice geometry constraints [1,3,4]. The exceptional magnetic properties of the latter systems attract particular theoretical [5–7] and experimental interest [8,9], aimed at the proper understanding of the cooperative paramagnetic state and the concurrent low-energy spectrum, while they have stimulated the search for materials exhibiting geometric frustration [10,11]. Recently, inelastic neutron scattering and magnetic susceptibility experiments revealed a frozen state of nanoscale spin clusters in the frustrated antiferromagnetic (AFM) $Zn_{1-x}Cd_xCr_2O_4$ spinels, characterized by extreme sensitivity to bond-disorder [12]. Moreover, the growth of AFM clusters far above the freezing temperature $T_f \approx 2.50$ K as well as the presence of spin clusters persisting below the collective freezing was earlier inferred in the Ga-diluted counterpart $ZnCr_{1.6}Ga_{0.4}O_4$, where site-disorder prevails [13].

Successful synthesis of the ternary vanadates $M_2FeV_3O_{11}$ (M=Zn, Mg) was recently reported during studies of phase equilibria in the MO-Fe_2O_3-V_2O_5 system [14,15]. Both compounds were found to crystallize in the triclinic system characterized by a non-statistical distribution of diamagnetic M^{2+} and high-spin Fe^{3+} ions, inferred from magnetic susceptibility measurements, on octahedral and bipyramidal sites [15]. In this work, the magnetic properties of $Zn_2FeV_3O_{11}$, whose crystal structure is determined by powder neutron diffraction, are studied using static magnetization and electron paramagnetic resonance (EPR) measurements. An inhomogeneous ground state is derived, involving a frozen, spin-glass-like state at low temperatures ($T_f \approx 2.5$ K) and the presence of large AFM spin clusters, both pertinent to the inherent cation disorder of the system.

2 Experimental

Polycrystalline samples of $Zn_2FeV_3O_{11}$ were prepared by the solid state reaction of a stoichiometric mixture of the ZnO, V_2O_3 and Fe_2O_3 oxides [14]. The sample was repetitively ground, pressed into pellets and calcined in air at 540 °C for 24 hrs and then at 640 °C for 24 hrs. At

[a] e-mail: ngouskos@cc.uoa.gr

each heating stage the sample was slowly cooled to room temperature, ground and analyzed by differential thermal analysis and X-ray diffraction (XRD), until the formation of single phase sample could be verified.

The crystal structure of the compound was investigated by neutron powder diffraction performed in the high luminosity DN-2 time-of-flight powder diffractometer at the Frank Laboratory of Neutron Physics of the Joint Institute for Nuclear Dubna Research (JINR) fast pulsed reactor, IBR-2. The neutron diffraction patterns were measured in the range of interplanar spacings d from 1 to 20 Å with resolution determined by the width of the pulse from the neutron source, $\Delta d/d = 0.01$. The diffraction patterns were collected at temperatures of 290 K, 100 K, and 15 K employing approximately 10 g of the sample enclosed in a thin-walled aluminium cylindrical container of 8 mm diameter.

Magnetization measurements were carried out using an MPMS-5 SQUID magnetometer in the temperature range of 2−300 K and magnetic fields up to 50 kOe in the zero-field-cooled (ZFC) and field-cooled (FC) modes. EPR measurements were carried out on powder samples sealed in quartz tubes using a Bruker E500 X-band spectrometer (ν = 9.45 GHz) with 100 kHz field modulation and magnetic field sweeps up to 14 kG. An Oxford flow cryostat was used for temperature dependent measurements (4−260 K).

3 Results and discussion

3.1 Crystal structure

Structure refinement was carried out using a computer program [16] based on the multi-phase Rietveld analysis method. The coherent neutron scattering lengths employed in the calculations were 5.680, 9.450, −0.3824, and 5.803 fm for Zn, Fe, V and O, respectively. A Gaussian function was chosen to generate the lineshape of the diffraction peaks, while the background was fitted to a fifth-order polynomial in d-spacing and refined simultaneously with the other profile parameters.

X-ray structural determination of $M_2FeV_3O_{11}$ (M=Zn, Mg) single crystals showed that both compounds are isostructural to $Zn_2GaV_3O_{11}$ [17], crystallizing in the triclinic space group $P-1$ [15]. There are three distinct crystallographic sites, where M and Fe atoms distribute non-statistically: the edge-sharing M(1) and M(2) octahedral sites and the bipyramidal M(3) one, which shares a corner with the $M(1)_2O_{10}$ octahedral dimer and one edge with the $M(2)O_6$ octahedron, as shown in Figure 1. A network built up from two types of VO_4 tetrahedra and the less common VO_5 trigonal bipyramid completes the crystal structure, where vanadium ions should be nominally in the diamagnetic V^{5+} state.

Room temperature structure refinements were accordingly performed taking as starting model the triclinic $Zn_2FeV_3O_{11}$ crystal structure with the distribution of Fe and Zn atoms confined in the M(1) and M(2) octahedral sites [15]. The results of the structural refinements are summarized in Table 1, where the results of the single-crystal X-ray determination (Ref. [15]) are also included. Good agreement between the observed and calculated diffraction profile was indeed obtained with lattice parameters close to those derived from the X-rays. However, similar results could be obtained allowing for different occupancies of the M(1), M(2), and M(3) sites by Zn and Fe atoms indicating that an unambiguous determination of the Zn/Fe disorder is not presently feasible, especially if the possibility of slight oxygen deficiency is taken into account. Most importantly, no evidence of long-range magnetic order could be detected from the neutron diffraction patterns at 15 K that show no magnetic Bragg peaks in the corresponding difference spectra.

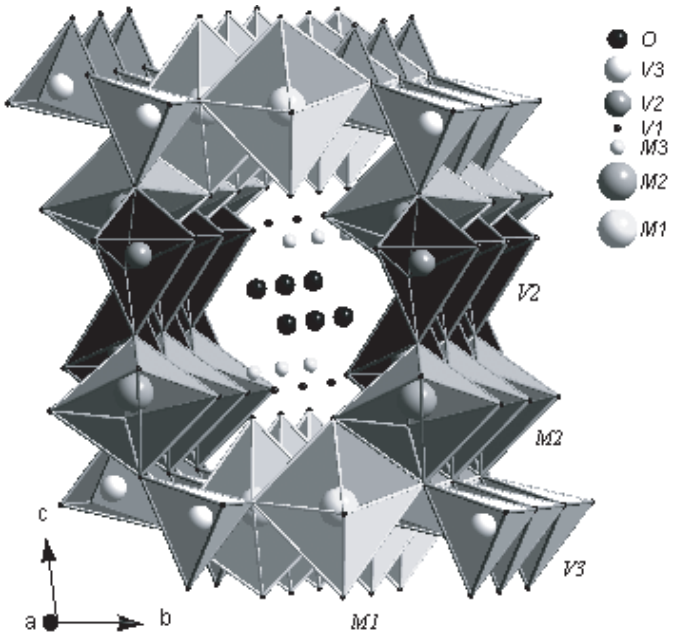

Fig. 1. Crystal structure of $Zn_2FeV_3O_{11}$.

3.2 Static magnetization

Figure 2 shows the temperature dependence of the inverse susceptibility χ^{-1}, derived from static magnetization measurements in the ZFC mode as M_{ZFC}/H. Curie-Weiss behavior can be evinced in two distinct temperature regimes. At $T > 50$ K, the Curie-Weiss fit to the $\chi^{-1}(T)$ data yields an effective moment of 5.45(1) μ_B per formula unit, which is close to the spin-only value of 5.92 μ_B of Fe^{3+} ions, and a negative Curie-Weiss temperature $\Theta = -58(1)$ K. Both values are close to those reported for $Zn_2FeV_3O_{11}$ in the temperature range of 50−300 K [15], indicating the presence of high-spin $3d^5$ iron. The value of the Weiss temperature suggests substantial AFM interactions, the strongest most likely occurring within the $M(1)_2O_{10}$ octahedral dimer with the shortest internuclear distance [M(1)-M(1) = 2.971 Å] and the edge sharing M(1) and M(2) octahedral sites [M(1)-M(2) = 3.215 Å] (Fig. 1). Such type of coupling complies with the Goodenough-Kanamori rules

Table 1. Structural parameters for $Zn_2FeV_3O_{11}$ obtained from the refinement of neutron powder diffraction data at room temperature with Fe and Zn atoms distributed in the M(1) and M(2) sites as M(1) = 0.639Fe+0.361Zn, M2 = 0.361Fe+0.639Zn, M3 = Zn, previously determined from single-crystal X-ray analysis (second column) [15]. Space group: $P-1$.

	Neutron diffraction	X-rays [15]
a (Å)	6.4538(5)	6.455(1)
b (Å)	6.8393(4)	6.834(1)
c (Å)	9.9924(7)	9.988(1)
α	97.556(9)°	97.65(1)°
β	102.650(8)°	102.61(1)°
γ	101.308(8)°	101.26(1)°
V (Å)^3	414.92	414.5
Z	2	2
M(1)		
x	0.3108(6)	0.3068(2)
y	0.8280(3)	0.8255(1)
z	0.5013(3)	0.4983(2)
M(2)		
x	0.2312(6)	0.2290(1)
y	0.4954(6)	0.4949(1)
z	0.2273(6)	0.2232(1)
M(3)		
x	−0.1766(6)	−0.1722(2)
y	0.1283(6)	0.1265(1)
z	0.1719(6)	0.1676(1)
R_p	3.54	-
R_w	2.62	-
χ^2	3.68	-

predicting predominantly AFM superexchange pathways for the d^5-d^5 pair interaction [18].

A paramagnetic-like downturn of χ^{-1} is observed at lower temperatures, a common feature of most frustrated antiferromagnets [1]. However, at $T<10$ K, the dc susceptibility exhibits a weak maximum at low fields with significant field dependence (inset of Fig. 2), suggestive of a spin-glass-like transition. To explore this behavior, the low-T dependence of the ZFC and FC magnetization was subsequently measured at different magnetic fields, as shown in Figure 3. The ZFC magnetization reveals a distinct cusp-like maximum in low fields ($H=10$ and 30 Oe) at $T\approx 2.5$ K, which practically coincides with the splitting of the $M_{\rm ZFC}$ and $M_{\rm FC}$ curves signaling the onset of irreversibility. At higher magnetic fields ($H>100$ Oe), the maximum becomes gradually smeared out, while the irreversibility onset shifts to lower temperatures, both indicative of a spin freezing transition. Figure 4 shows the temperature derivative of $M_{\rm ZFC}$ as a function of temperature for various magnetic fields. The freezing temperature T_f can be clearly identified from the center of the resonance-like curve at 2.55 K, where all plots of the tem-

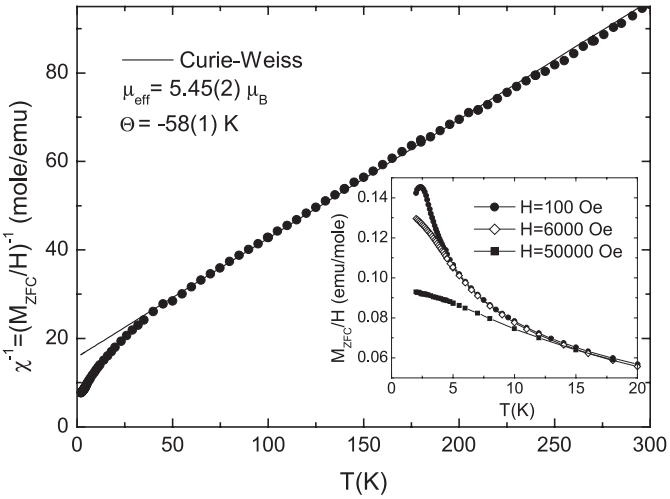

Fig. 2. Temperature dependence of the inverse dc susceptibility, defined as $\chi^{-1}=(M_{\rm ZFC}/H)^{-1}$, for $Zn_2FeV_3O_{11}$. The solid line shows the Curie-Weiss fit at high temperatures ($T>50$ K). The inset shows in detail the field dependence of $M_{\rm ZFC}/H$ at $T<20$ K.

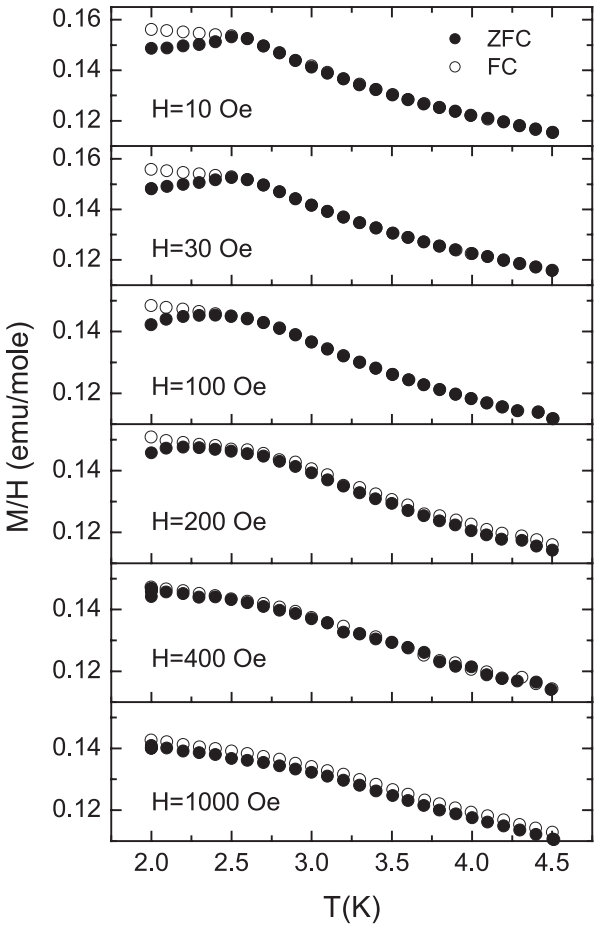

Fig. 3. Low temperature dependence of the ZFC and FC magnetization M/H for $Zn_2FeV_3O_{11}$ at magnetic fields up to 1000 Oe.

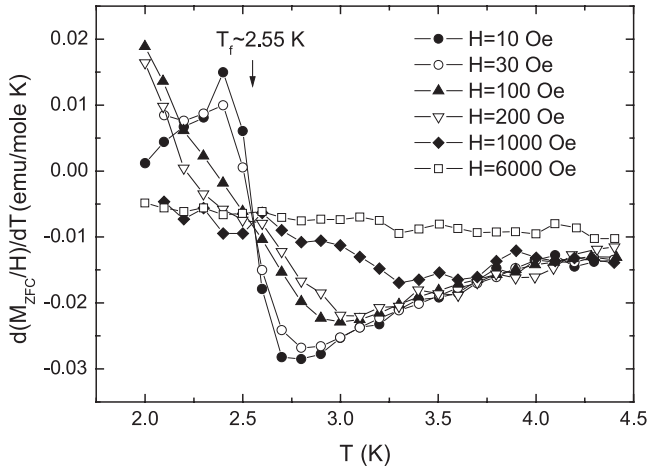

Fig. 4. Plots of the temperature derivative $d(M_{\rm ZFC}/H)/dT$ vs. T at low temperatures for different applied fields. The arrow identifies the freezing temperature $T_f = 2.55$ K from the crossing point of all curves.

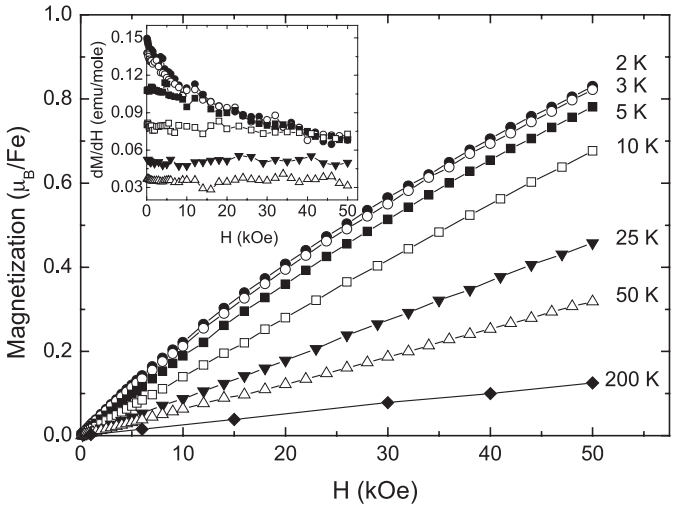

Fig. 5. Field dependence of the dc magnetization for $Zn_2FeV_3O_{11}$ at different temperatures. The inset shows the corresponding field dependence of the differential magnetic susceptibility dM/dH.

perature derivative $d(M_{\rm ZFC}/H)/dT$ vs. T cross for different applied fields [19].

Comparison of the Curie-Weiss temperature that sets up the mean-field energy scale for the AFM pairwise coupling of Fe^{3+} spins and the freezing temperature yields the ratio $f = -\Theta/T_f \approx 23$, suggesting significant spin frustration [1] as well as appreciable AFM correlations in the paramagnetic phase. It is worth noting that an accurate description of $\chi^{-1}(T)$ can be obtained from 300 K down to 3 K, by fitting to a two component Curie-Weiss expression, similar to many geometrically frustrated antiferromagnets [5]. Such a phenomenological description would reflect the presence of two separate spin populations, one stemming from the strongly correlated spins and the other one due to a small fraction of uncorrelated "orphan" spins.

Figure 5 shows the field dependence of the isothermal dc magnetization $M(H)$ at various temperatures. The low magnetization at 2 K, sustained up to 50 kOe, asserts the strong AFM coupling and the concurrent compensation of a large fraction of Fe^{3+} moments. The field dependence of the differential susceptibility dM/dH, numerically calculated from the $M(H)$ data (inset of Fig. 5), confirms the flattening of $\chi(T)$ at high magnetic fields and the small curvature of the $M(H)$ curves at low-T. The latter behavior, which is contrary to that of conventional antiferromagnets, complies qualitatively with the presence of a small fraction of relatively uncompensated spins or even AFM clusters with reduced energy gap at low temperatures.

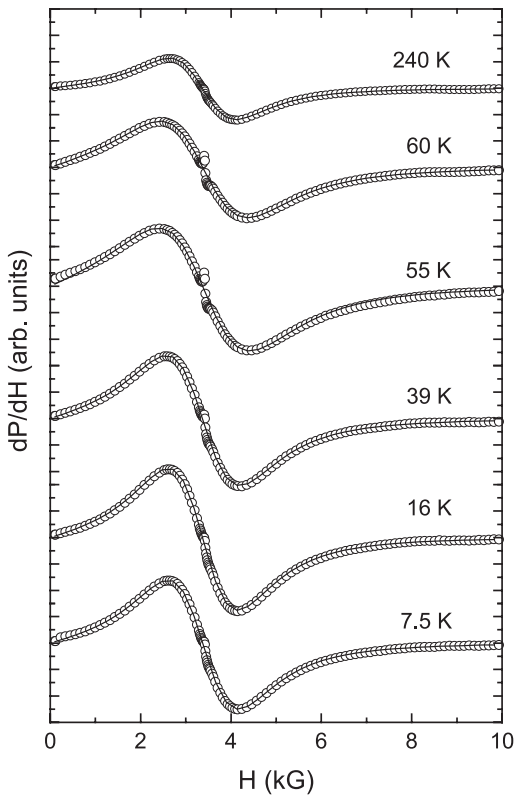

Fig. 6. Temperature dependence of the EPR spectra for $Zn_2FeV_3O_{11}$ at the X-band ($\nu \approx 9.45$ GHz). Solid lines show the best-fit curves to a single Lorentzian lineshape.

3.3 Electron paramagnetic resonance

Figure 6 shows representative EPR spectra of $Zn_2FeV_3O_{11}$ at different temperatures. A single, broad resonance line in the $g \approx 2.0$ region dominates the spectra in the whole temperature range, while a much weaker and narrow resonance line is observed at $g \approx 2.02(1)$, most probably due to paramagnetic defects. To explore the origin of the resonance line, the EPR susceptibility $\chi_{\rm EPR}$ was estimated by double integration of the absorption derivative over a field range of 10 ΔH_{pp} (peak-to-peak linewidth) at 260 K and comparison to that of weighted $CuSO_4{\cdot}5H_2O$ reference samples [20]. The value of 0.008(3) emu/mole is found for $\chi_{\rm EPR}$ at 260 K, which corresponds to about 70% of the

static susceptibility $\chi(260\ \mathrm{K}) = 0.0118(1)$ emu/mole and approximately $5.5(3) \times 10^{20}$ spins/g assuming the presence of Fe^{3+} ions in the high-spin state ($S = 5/2$). This could be partly explained by the limited accuracy of χ_{EPR}, as well as that a fraction of Fe^{3+} spins detected by the static susceptibility may not contribute to the resonance line, complying further with the presence of AFM correlations from high temperatures, previously inferred from the static magnetic data. To evaluate the temperature variation of the EPR parameters, the derivative spectra were fitted to a full Lorentz line comprising the tail of the resonance absorption at negative field, a consequence of the linearly polarized rf field that is important when the width becomes comparable to the resonance field. Accurate fitting was thus obtained (Fig. 6) indicating that exchange narrowing is effective in the whole T-range.

Figure 7 summarizes the temperature dependence of the EPR parameters, namely the EPR susceptibility χ_{EPR} and the product of $\chi_{\mathrm{EPR}}T$, the linewidth ΔH (half-width at half-height) and the effective g-factor. At high temperatures ($T > 70$ K), the EPR susceptibility is considerably reduced compared with the paramagnetic behavior $\sim 1/T$ of Fe^{3+} spins resembling the temperature variation of the static $\chi(T)$. This can be most readily observed in the comparative plots of $\chi_{\mathrm{EPR}}T$ vs. T and χT vs. T included in the inset of Figure 7a, where a continuous decrease is detected in accordance with the Curie-Weiss law for both cases. However, a weak but well defined peak of $\chi_{\mathrm{EPR}}(T)$ is observed at $T \approx 55$ K, very close to the Curie-Weiss temperature determined from the high-T static susceptibility. At lower temperatures ($T < 40$ K), $\chi_{\mathrm{EPR}}(T)$ remains approximately constant, followed by a small decrease below 15 K, while $\chi_{\mathrm{EPR}}T$ becomes approximately 50% of the high-T value and then decreases continuously down to low temperatures, suggesting that AFM correlations are operative. In the same temperature range, ΔH increases continuously down to $T \approx 55$ K, where a peak is observed, concurrently with $\chi_{\mathrm{EPR}}(T)$, and then decreases steeply towards the high-temperature value [Fig. 7b]. Moreover, a clearly detectable temperature variation of the g-factor that reaches a minimum value close to 55 K, is also observed [Fig. 7c].

Such a temperature variation of the EPR parameters is frequently observed near magnetic phase transitions for ordinary antiferromagnets [21] or spin-glasses [22], due to the slowing down of spin fluctuations and the growth of internal fields. Nevertheless, critical broadening may not be necessarily invoked, since the pronounced temperature dependence of the product $(\chi T)^{-1}$ reflecting the presence of strong AFM correlations from high temperatures [23], might also account for the $\Delta H(T)$ variation up to 55 K [Fig. 7b] provided that AFM ordering occurs at that temperature. However, no evidence of long-range order could be observed at 55 K by both static magnetization and neutron diffraction measurements rendering analysis in terms of the EPR response of antiferromagnetic systems above T_N most likely inappropriate.

Discrepancy between the temperature decrement of the dc susceptibility and χ_{EPR} was recently observed for

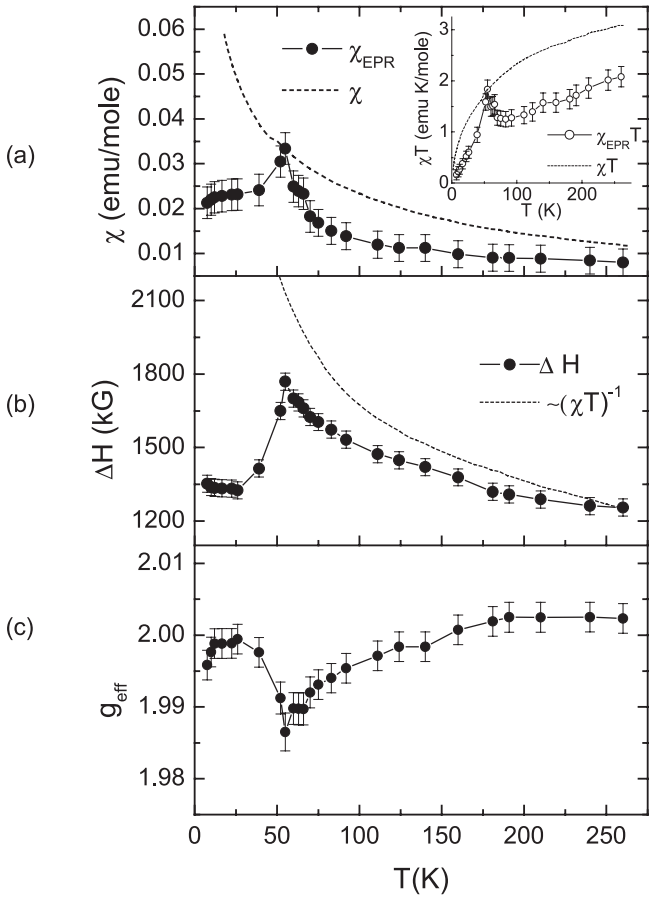

Fig. 7. Temperature dependence of the (a) EPR χ_{EPR} (symbols) and static χ (dashed line) susceptibilies, (b) linewidth ΔH (symbols) compared with the temperature dependence of $(\chi T)^{-1}$ (dashed line), and (c) the effective g-factor for $Zn_2FeV_3O_{11}$. The inset in (a) compares the product of $\chi_{\mathrm{EPR}}T$ with χT.

the frustrated AFM spinel $ZnCr_2O4$, which was analyzed by taking into account transitions from the excited states of Cr^{3+} spin-coupled pairs [24]. However, neither $g(T)$, which was temperature independent, nor $\Delta H(T)$, which broadened continuously towards T_N, showed any anomalous variation at intermediate temperatures. A maximum of $\Delta H(T)$ and $\chi_{\mathrm{EPR}}T$ has been reported at T_f for the insulating thiospinels $CdIn_{2-2x}Cr_{2x}S_4$ pertaining mostly to the presence of competing ferromagnetic and antiferromagnetic interactions [25], whereas a continuous temperature variation of the EPR parameters has been detected for the purely AFM oxispinel $ZnCr_{1.6}Ga_{0.4}O_4$ [13]. The assignment of the EPR line to the discrete energy spectrum of isolated AFM spin-clusters, such as Fe^{3+} pairs, with enhanced exchange integrals of the order of $J/k_B \approx 50$ K, may likewise account for the maximum of $\chi_{\mathrm{EPR}}(T)$. Nevertheless, thermal depopulation of the excited spin states of the Fe^{3+} pairs or even larger spin-clusters would lead to a smooth variation of χ_{EPR} over a wider temperature range rather than the anomalous peak at $T \approx 55$ K. Similar behavior would be also anticipated for the static

susceptibility that reflects the contribution of all possible spin states. A magnetically inhomogeneous state can be thus suggested, where the contribution of clusters with the stronger AFM coupling should be relatively small and most importantly superimposed on a sizable AFM background characterized by reduced exchange interactions. The latter contribution should prevail down to low temperatures, eventually leading to the formation of the frozen state at $T_f = 2.55$ K. The concomitant divergence of $\Delta H(T)$ and $g(T)$ at ≈ 55 K due to these isolated spin-clusters would be difficult to explain, unless we allow for the contribution of unresolved fine structure transitions of the excited spin states which shift and broaden effectively the whole EPR spectrum.

On the other hand, a more plausible picture of the ground state can be suggested, assuming that at high temperatures exchange coupled Fe^{3+} spins occupying the M(1) and M(2) sites contribute to the EPR signal, while at lower temperatures short range AFM order, confined in distinct spatial regions, results in an inhomogeneous resonance line. The EPR line would then originate from two separate spin systems, one due to large AFM clusters and the other due to regions with reduced exchange interactions. The former system characterized by an energy gap of the order of 50 K, whose contribution becomes rapidly wiped out from the EPR line, may then explain the steep variation of all the EPR parameters, namely the reduction of $\chi_{\rm EPR}$, the g-shift and the divergent behavior of ΔH in the relatively narrow temperature range of 40−60 K. Below 40 K, the remaining Fe^{3+} spins would dominate the EPR signal, though antiferromagnetic correlations are still effective leading to the spin freezing transition at low temperatures. It is worth noting that the magnetic inhomogeneity may be further promoted by the presence of oxygen deficiency and a small fraction of magnetic vanadium spins (e.g. V^{4+} with spin $S = 1/2$) that may disrupt or enhance the exchange coupling of Fe^{3+} moments.

4 Conclusions

In conclusion, dc magnetization and EPR measurements on the recently synthesized ternary vanadate $Zn_2FeV_3O_{11}$ provide experimental evidence for the presence of significant magnetic frustration due to the inherent site-disorder of Fe^{3+} spins. In particular, the dc magnetic susceptibility indicates low-temperature spin freezing at $T_f = 2.55$ K, in contrast with the presence AFM correlations appearing from high temperatures. EPR measurements confirm the presence of strong AFM interactions and most remarkably reveal divergent variation of all the EPR parameters at $T \approx 55$ K, coinciding with the mean-field energy scale provided by the Curie-Weiss temperature $\Theta \approx -58$ K. This behavior is mainly attributed to the magnetic inhomogeneous state of the system comprising AFM clusters due to short-range ordered Fe^{3+} spins with an energy gap of the order of 50 K as well as regions with reduced exchange interactions.

References

1. A.P. Ramirez, Annu. Rev. Mater. Sci. **24**, 453 (1994)
2. K. Binder, A.P. Young, Rev. Mod. Phys. **58**, 801 (1986)
3. P. Schiffer, A.P. Ramirez, Comments Condens. Matter Phys. **18**, 21 (1996)
4. J.E. Greedan, J. Mater. Chem. **11**, 37 (2001)
5. P. Schiffer, I. Daruka, Phys. Rev. B **56**, 13 712 (1997)
6. R. Moessner, A.J. Berlisnky, Phys. Rev. Lett. **83**, 3293 (1999)
7. A.J. Garcia-Adeva, D.L. Huber, Phys. Rev. B **65**, 184418 (2002)
8. A.P. Ramirez, B. Hessen, M. Winklemann, Phys. Rev. Lett. **84**, 2957 (2000)
9. L. Limot, P. Mendels, G. Colin, C. Mondelli, B. Ouladdiaf, H. Mutka, N. Blanchard, M. Mekata, Phys. Rev. B **65**, 144447 (2002)
10. N. Rogado, G. Lawes, D.A. Huse, A.P. Ramirez, R.J. Cava, Solid State Commun. **124**, 229 (2002)
11. C.R. Wiebe, J.E. Greedan, G.M. Luke, J.S. Gardner, Phys. Rev. B **65**, 144413 (2002)
12. W. Ratcliff II, S.-H. Lee, C. Broholm, S.-W. Cheong, Q. Huang, Phys. Rev. B **65**, 220406(R) (2002)
13. D. Fiorani, S. Viticoli, J.L. Dormann, J.L. Tholence, A.P. Murani, Phys. Rev. B **30**, 2776 (1984)
14. I. Rychlowska-Himmel, A. Blonska-Tabero, J. Therm. Anal. Cal. **56**, 205 (1999)
15. X. Wang, D.A. Vander Griend, C.L. Stern, K.P. Poeppelmeier, J. Alloys Comp. **298**, 119 (2000)
16. V.B. Zlokazov, V.V. Chernyshev, J. Appl. Crystallogr. **25**, 447 (1992)
17. C. Müller, H. Müller-Buschbaum, J. Alloys Comp. **191**, 251 (1993)
18. A.P. Ginsberg, Inorg. Chim. Acta Rev. **5**, 45 (1971)
19. R.V. Chamberlin, M. Hardiman, L.A. Turkevich, R. Orbach, Phys. Rev. B **25**, 6720 (1982)
20. C.P. Poole, *Electron Spin Resonance*, 2nd edn. (Wiley-Interscience, New York, 1983)
21. D.L. Huber, Phys. Rev. B **6**, 3180 (1972)
22. C.Y. Huang, J. Magn. Magn. Mater. **51**, 1 (1985)
23. E. Dormann, V. Jaccarino, Phys. Lett. A **48**, 81 (1974)
24. H. Martinho, N.O. Moreno, J.A. Sanjurjo, C. Rettori, A.J. Garcia-Adeva, D.L. Huber, S.B. Oseroff, W. Ratcliff II, S.-W. Cheong, P.G. Pagliuso, J.L. Sarrao, G.B. Martins, Phys. Rev. B **64**, 024408 (2001)
25. S. Viticoli, D. Fiorani, M. Nogués, J.L. Dormann, Phys. Rev. B **26**, 6085 (1982)